http://dx.doi.org/10.5516/NET.04.2012.516

CRITICAL HEAT FLUX ENHANCEMENT IN FLOW BOILING OF Al_2O_3 AND SiC NANOFLUIDS UNDER LOW PRESSURE AND LOW FLOW CONDITIONS

SEUNG WON LEE[1], SEONG DAE PARK[1], SARAH KANG[1], SEONG MAN KIM[1], HAN SEO[1], DONG WON LEE[2], and IN CHEOL BANG[1*]

[1]Interdisciplinary School of Green Energy, Ulsan National Institute of Science and Technology (UNIST),
100 Banyeon-ri, Eonyang-eup, Ulju-gun, Ulsan Metropolitan City, Republic of Korea 689-798

[2]Korea Atomic Energy Research Institute (KAERI)
Deokjin-dong, Yuseong-gu, Daejeon, Republic of Korea 305-600

[*]Corresponding author. E-mail : icbang@unist.ac.kr

Invited September14, 2011
Received October 30, 2011
Accepted for Publication February 27, 2012

Critical heat flux (CHF) is the thermal limit of a phenomenon in which a phase change occurs during heating (such as bubbles forming on a metal surface used to heat water), which suddenly decreases the heat transfer efficiency, thus causing localized overheating of the heating surface. The enhancement of CHF can increase the safety margins and allow operation at higher heat fluxes; thus, it can increase the economy. A very interesting characteristic of nanofluids is their ability to significantly enhance the CHF. Nanofluids are nanotechnology-based colloidal dispersions engineered through the stable suspension of nanoparticles. All experiments were performed in round tubes with an inner diameter of 0.01041 m and a length of 0.5 m under low pressure and low flow (LPLF) conditions at a fixed inlet temperature using water, 0.01 vol.% Al_2O_3/water nanofluid, and SiC/water nanofluid. It was found that the CHF of the nanofluids was enhanced and the CHF of the SiC/water nanofluid was more enhanced than that of the Al_2O_3/water nanofluid.

KEYWORDS : Critical Heat Flux, Flow Boiling, Nanofluids, Low Pressure and Low Flow

1. INTRODUCTION

Critical heat flux (CHF) is characterized by a sudden reduction of the local heat transfer coefficient (HTC) that results from the replacement of liquid by vapor adjacent to the heat transfer surface [1]. Ordinarily, the CHF represents a thermal limitation in which a phase change occurs during heating. When the CHF occurs, an inordinate decrease in the heat transfer rate for both the heat flux and temperature controlled systems is generated. This is generally more important in applications such as power generation for heat flux controlled systems, due to the burnout or integrity failure that occurs on heated surface. Thus, it is very important to enhance the CHF in order to ensure system safety and to improve efficiency.

Many methods of enhancing the CHF have been investigated, e.g. the swirl flow using twisted tapes, the promotion of flow mixing, the altering of the heated surface characteristics, and the changing of the surface tension; in recent years, a new technique has been proposed using nanofluid technology. Nanofluids are nanotechnology-based fluids engineered to enhance thermal conductivity through dispersing and stably suspending nanoparticles in traditional heat transfer fluids [2]. One of the most interesting characteristics of nanofluids is their ability to significantly enhance the CHF.

The primary objective of the present research is to do CHF enhancement experiments in flow boiling using nanofluids under low pressure and low flow (LPLF) conditions. Some CHF experiments relevant to the present work for flow boiling include the following. Chang et al. [3] investigated the stable flow of water in vertical tubes in low pressure and velocity conditions. Experiments were performed using round tubes with diameters of 0.006 m and 0.0088 m for mass fluxes below 200 kg/m^{2}s under atmospheric pressure. A new design correlation was proposed based on the combination of the present data and other CHF data available in the literature. Assessments of the experiments demonstrate reasonable agreement between the predictions and the experiments. Kim et al. [4] performed water flow in vertical round tubes under LPLF conditions in order to provide a systematic database and to investigate parametric trends. A total of 513 sets of experimental data were obtained using Inconel-625 tube

test sections in the following conditions. Test sections with four (6, 8, 10, and 12 mm) diameters and variable lengths were used for the experiment at low pressure (P = 106~951 kPa) and low flow (G = 20~277 kg/m^{2}s) conditions. Kim et al. [5] studied flow boiling CHF in nanofluids. They used a 0.01 vol.% alumina nanofluid characterized by nanoparticles with a size of ~50 nm. The results demonstrate that CHF enhancement up to ~30 % can be achieved using the nanofluid. Kim et al. [6] showed that the maximum CHF enhancements were 53 %, 53 %, and 38 % for alumina, zinc oxide, and diamond nanofluids, respectively. They concluded that an analysis of the boiling surface reveals that its morphology is altered by the deposition of the particles during boiling. Additionally, the wettability of the surface is substantially increased, which appears to correlate well with the observed CHF enhancement. Kim et al. [7] performed flow boiling CHF experiments using an Al_2O_3 nanofluid at different inlet temperatures (50 and 75 °C) and mass fluxes (100, 200, and 300 kg/m^{2}s). The CHF results for water agreed well with the results provided in the 1995 CHF look-up table prepared by Groeneveld. The results demonstrated that the CHFs of the Al_2O_3 nanofluids were enhanced up to ~70 % in flow boiling for all experimental conditions. The inner surfaces of the test section tube were observed using an FE-SEM and the zeta potentials of the Al_2O_3 nanofluids were measured before and after the CHF experiments. Most CHF experiments were conducted using Al_2O_3 nanofluids with low subcooling and were compared with the 1995 Groeneveld results in a look-up table [8].

SiC is considered as a candidate for wall materials of fusion reactors, in which a high temperature and high radiation environment is expected. Also, SiC has demonstrated its potential as a coating material for use as a high temperature gas cooled reactor fuel. Thus, the resistance of SiC to high temperature and high radiation environments can provide a good reason for applying SiC as a cladding material for light water nuclear reactors [9]. Therefore, this work was performed to provide CHF data using SiC/water nanofluids as well as Al_2O_3/water nanofluids for LPLF conditions with high subcooling (inlet temperature: 25 and 50 °C) and to compare the obtained results with the 2006 Groeneveld look-up table [10].

2. EXPERIMENT

2.1 Preparation of Al_2O_3/Water and SiC/Water Nanofluids

The nanoparticles/water nanofluids were prepared by dispersing the nanoparticles into water as a base fluid. The Al_2O_3 nanoparticles (true density = 3970 kg/m^3, thermal conductivity = 40 W/(mK)) in this study were manufactured by Alfa Aesar, Johnson Matthey Company. The SiC nanoparticles (true density = 3160 kg/m^3, thermal conductivity = 490 W/(mK)) were manufactured by Sigma Aldrich. It is well known that the nanofluid properties depend on the shape and size of the nanoparticles. In order to identify the nanofluid morphology, a transmission electron microscopy (TEM) was performed. As can be seen in the image in Fig. 1, it was identified that the Al_2O_3 and SiC nanoparticles have spherical shapes. The size of the Al_2O_3 nanoparticles was smaller than 50 nm and that of the SiC nanoparticles was larger than 50 nm.

The preparation process for the nanoparticles/water nanofluids is as follows: (1) weigh the nanoparticle mass using a digital electronic balance; (2) put the nanoparticles into weighed water and prepare the nanoparticles/water mixture; and (3) sonicate the mixture continuously for six hours using a sonicator in order to obtain uniform dispersion of the nanoparticles in the water. Through this preparation, the temperature of the nanofluids increased from 24 °C to 55 °C [11].

In the present work, 0.01 vol.% Al_2O_3/water and SiC/water nanofluid was prepared. In terms of the colloidal stability or stable nanoparticle-dispersion, the zeta potential is a key parameter. The zeta potential of the Al_2O_3/water nanofluid was +36 mV and that of the SiC/water nanofluid was -37.3 mV (Fig. 2). It can be seen that these values show moderate stability, because the absolute values of the zeta potential are larger than 30 mV. In terms of the colloidal stability or stable nanoparticle dispersion, the pH is a key parameter that is related to the electrostatic charge on the

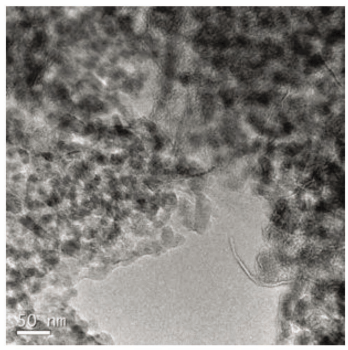

(a)

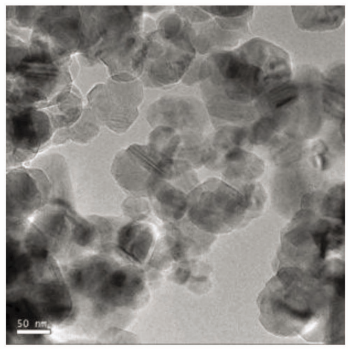

(b)

Fig. 1. TEM Images of the Nanoparticles: (a) Al_2O_3 and (b) SiC.

particles surface. This can be interpreted and quantified as the zeta potential. It is well known that the pH value required in order to maintain stability must be far from the isoelectric point (IEP), which is the pH at which a particle surface does not have a net electrical charge (zero zeta potential). Therefore, in a colloidal dispersion, the IEP brings about the precipitation and agglomeration of particles because there are insufficient repulsive forces between the particles. As the pH changes from the IEP, the absolute value of the zeta potential of the particle surface increases so that the interaction between the particles due to the existence of the electrical double layer (EDL) becomes sufficient to prevent attraction and collision between particles caused by the Brownian motion.

2.2 CHF Experiment

The influences of the Al_2O_3/water and SiC/water nanofluids and the fluid thermal hydraulic conditions (mass flux) on the CHF have been determined through experiments in the flow boiling loop that is shown in Fig. 3. Experiments were performed using 1/2 inch stainless steel 316L (test section length: 0.5 m) with mass flux values of 100, 150, 200, and 250 kg/m^{2}s and inlet temperatures of 25 and 50 °C. The main components of the experimental system include an overhead liquid reservoir (working fluid storage and prevention of countercurrent), a surge tank (working fluid storage), a magnet turbine pump (the working fluids were circulated using a pump with a variable speed driver), a pre-heater to control the inlet temperature of the working fluid, a flow meter to confirm the flow mass rate of the working fluid (the uncertainty of the flow mass rate was less than ±4 %), a test section, a DC power supply, and a condenser for cooling the working fluid. The test section was installed in order to adjust the angle; that is, the test section can be vertical and horizontal, and is determined in a flexible way. Two piezoresistive transmitters were installed at the inlet and exit of the test section in order to monitor the pressure of the test section inlet and exit. Also, ten thermocouples were installed in order to monitor the temperature of the test section part, test section inlet and exit, tank, and condenser exit. The test section was directly heated using a 75 kW (30 V, 2500 A) DC power supply. (the uncertainty of the power supplied to the test section

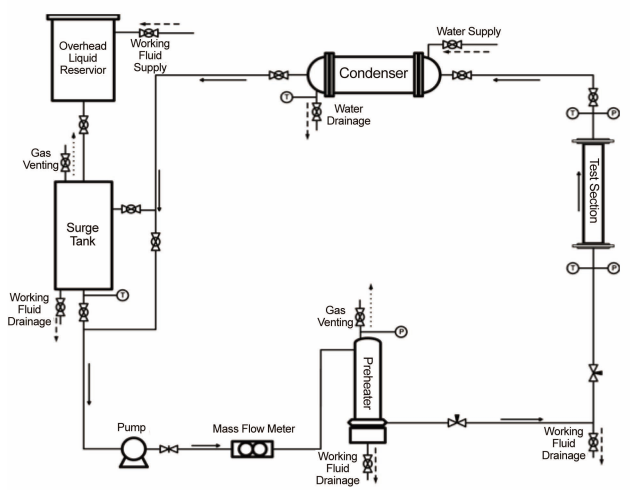

Fig. 3. Schematic Diagram of the Flow Boiling Loop.

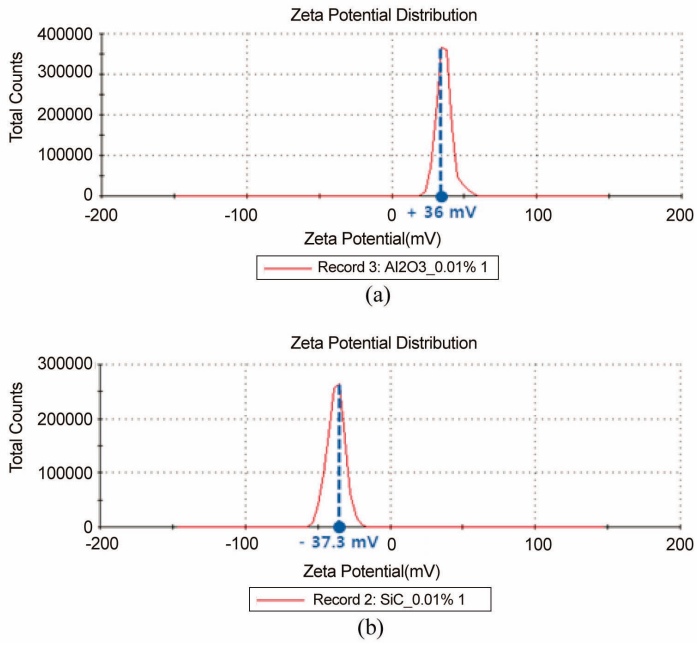

Fig. 2. Zeta Potential of 0.01 vol.% Nanofluids: (a) Al_2O_3/Water Nanofluid and (b) SiC/Water Nanofluid.

was measured using a multimeter to be less than 1.5 %). Also, an Agilent data acquisition system was used to read the individual instrument outputs and translate them into physical parameters. A computer was used to sample all data periodically and to monitor the experiment.

The experimental procedure was as follows. The working fluid was flowed by a pump and heated by a pre-heater in order to remove the non-condensable gas and to adjust the inlet temperature. The voltage was increased stepwise until the CHF occurred [12]. The experiment was performed twice for each condition (water, Al_2O_3/water, and SiC/water nanofluids with smooth tubes). The total amount of each fluid was 74 liters. All experiments were performed in flow boiling under atmospheric pressure at fixed inlet temperatures (25 and 50 °C) and fixed mass fluxes (100, 150, 200, and 250 kg/m^{2}s).

The calculation of the heat flux in the test section is as follows:

$$q'' = \frac{VI}{\pi D_{inner} L} \quad , \tag{1}$$

where V is the measured voltage, I is the measured current, D_{inner} is the inner diameter of the test section (1/2 inch stainless steel 316 L tube), and L is the length of the test section.

The CHF results for water were compared with the 2006 CHF look-up table prepared by Groeneveld [10]. In comparison with the 2006 Groeneveld look-up table, the critical steam quality was calculated using the heat balance equation for the first action. Heat losses in the test section were less than 9 % for an increasing heat flux of 100~3500 kW/m^2 (for an increasing voltage of 4~25 V).

The heat balance equation is as follows:

$$X_{cr} = \frac{1}{h_{fg}}\left[\frac{4q''z}{DG} - (\Delta h_{sub})_{inlet}\right], \tag{2}$$

where X_{cr} is the critical steam quality, h_{fg} is the latent heat of vaporization (MJ/kg), q'' is the critical heat flux (MW/m^2), z is the tube length (m), D is the tube diameter (m), G is the mass flux (kg/m^{2}s), and $(\Delta h_{sub})_{inlet}$ is the enthalpy inlet subcooling (MJ/kg).

3. RESULTS AND DISCUSSION

In a gas-liquid, the two phases can adopt various geometric configurations known as flow patterns or flow regimes. As the quality is gradually increased from zero, the common flow regimes for vertical upflow, which is where both phases flow upwards in a circular tube, are bubbly flow, plug flow, churn flow, and annular flow. Flow pattern maps attempt to separate the space into areas corresponding to the various flow patterns using a two-dimensional graph [13]. The commonly useful flow pattern maps are the Baker map [14], the Hewitt and Roberts map [15], and the Taitel and Dukler map [16].

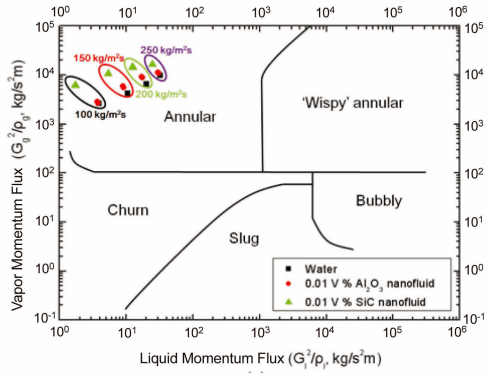

(a)

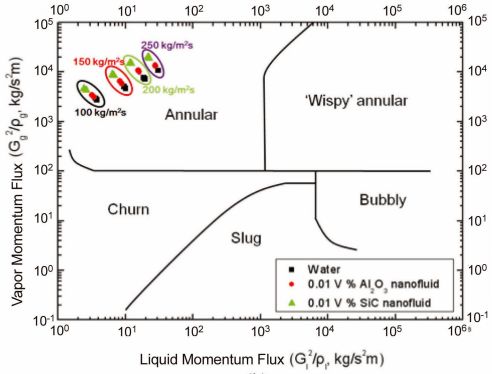

(b)

Fig. 4. Hewitt and Roberts Flow Regimes map (1969) for the CHF Data According to the Inlet Temperature: (a) T_{in}: 25 °C and (b) T_{in}: 50 °C.

Among these flow pattern maps, the Hewitt and Roberts flow regimes for vertical flow were investigated using the experimental results, as shown in Fig. 4. In this figure, G^2/ρ is the momentum flux and all transitions are assumed to depend on the phase momentum fluxes. 'Wispy' annular flow is a sub-category of annular flow that occurs at a high mass flux when the entrained drops appear as wisps or elongated droplets [15]. The flow regimes in all conditions (inlet temperature: 25 and 50 °C; mass flux: 100, 150, 200, and 250 kg/m^{2}s; working fluid: water, Al_2O_3/water nanofluid, and SiC/water nanofluid) were annular flows. Annular flows are when the liquid moves as an annular film on the inner surface of the tube and the tiny drops distributed in the gas move to the center of the tube. The mechanism that occurs in the CHF is a liquid film dryout (LFD) in the annular flow regime. The CHF condition was decided when the maximum surface temperature exceeded 200 °C with a rapid increase, because the mechanism that occurs in the CHF is the LFD, as shown in Fig. 5. This condition was confirmed through observations that the surface temperature of the tube increased rapidly when it exceeded 200 °C.

For fixed inlet conditions, the parametric trends of the CHF are mass flux, diameter, heated length, inlet subcooling,

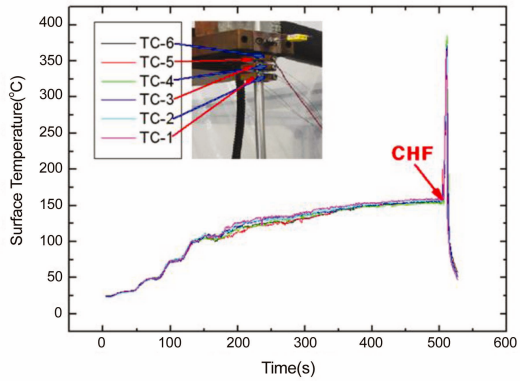

Fig. 5. Surface Temperature of the Test Section near the CHF.

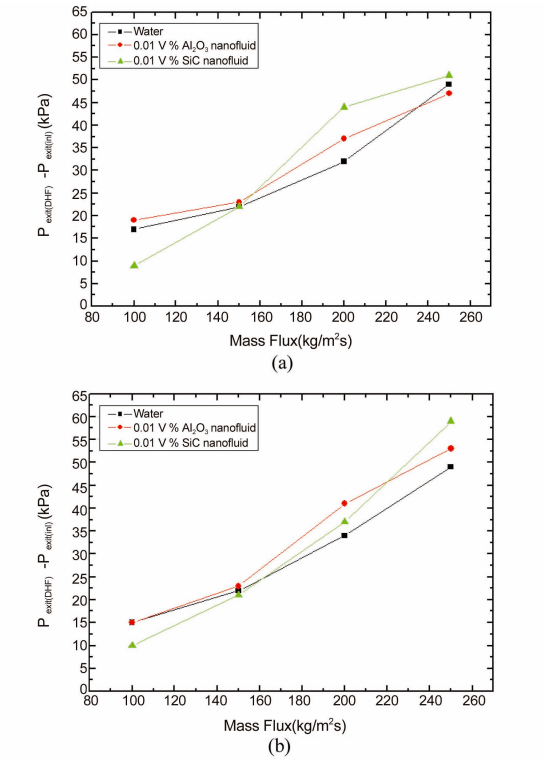

Fig. 6. Pressure Difference with Different Mass Fluxes According to the Inlet Temperature: (a) T_{in}: 25 °C and (b) T_{in}: 50 °C.

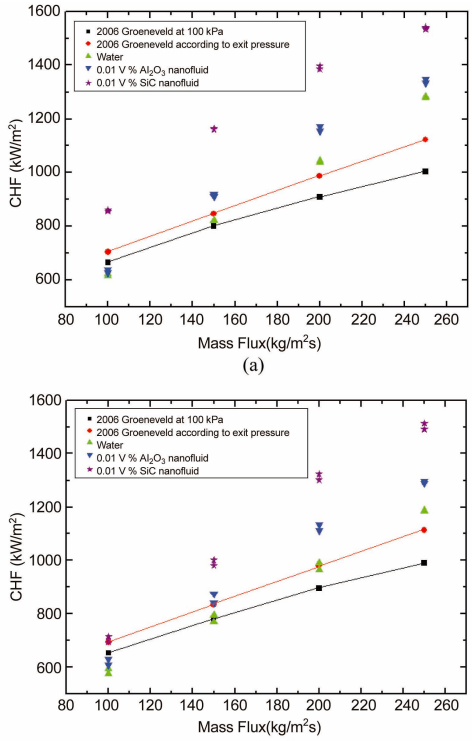

Fig. 7. CHF Data with Different Mass Fluxes According to the Inlet Temperature: (a) T_{in}: 25 °C and (b) T_{in}: 50 °C.

and pressure. The pressure among these parameters is known to result in the increase of the CHF, which occurs according to the increase in the pressure [17, 18]. Moreover, Moon et al. [19] demonstrated that the pressure had an opposite trend for the LPLF conditions; Kim et al. [4] revealed that the CHF slowly increased with pressure increases for higher mass fluxes, but that the effect becomes negligible at lower mass fluxes. In the present work, the pressure at the test section exit increased according to the increase of the mass flux, as shown in Fig. 6, despite maintaining a constant fluid level in the overhead liquid reservoir. In Fig. 6, the difference between the initial exit pressure and exit pressure at which the CHF occurs resulted from the change in initial exit pressure when each experiment was performed. That is, the exit pressure at which the CHF occurred is almost the same according to the working fluids. Although the difference of the initial exit pressure and exit pressure at which the CHF occurs increased as the mass flux increased, the CHF increased slightly according to the pressure because the exit pressure at which the CHF occurred was nearly the same according to the mass flux increase for water, Al_2O_3/water nanofluid, and SiC/water nanofluid.

The CHF results for water were similar to those in the 2006 Groeneveld look-up table, as shown in Fig. 7. In this figure, the black line is the 2006 Groeneveld data at 100 kPa and the red line is the 2006 Groeneveld data according to the exit pressure. Furthermore, the CHF results for the Al_2O_3/water and SiC/water nanofluids were enhanced through the increase of the mass flux at inlet temperatures of 25 °C and 50 °C; the CHF results for the SiC/water nanofluid were more enhanced than those for the CHF for the Al_2O_3/water nanofluid in all experiment conditions. As seen in Fig. 8, the CHF enhancement ratios of the Al_2O_3/water and SiC/water nanofluids did not increase with an increase in the mass flux at inlet temperatures of 25 °C and 50 °C because the deposition structure of the nanoparticles according to the mass flux is different. For

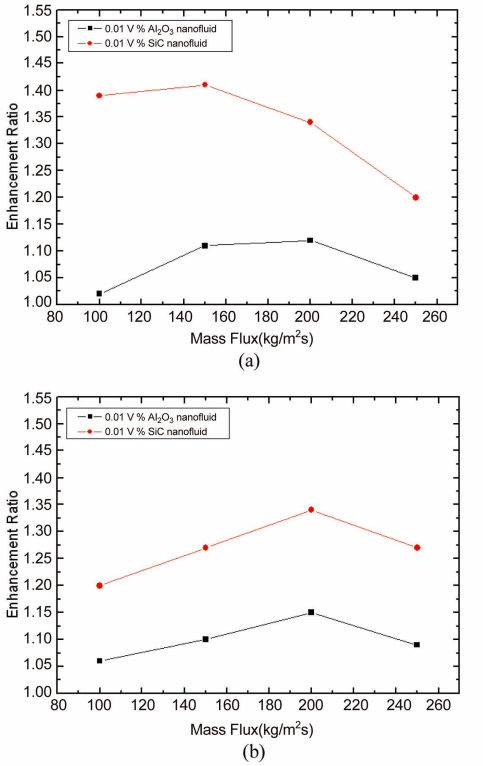

Fig. 8. CHF Enhancement Ratios with Different Mass Fluxes According to the Inlet Temperature: (a) T_{in}: 25 °C and (b) T_{in}: 50 °C.

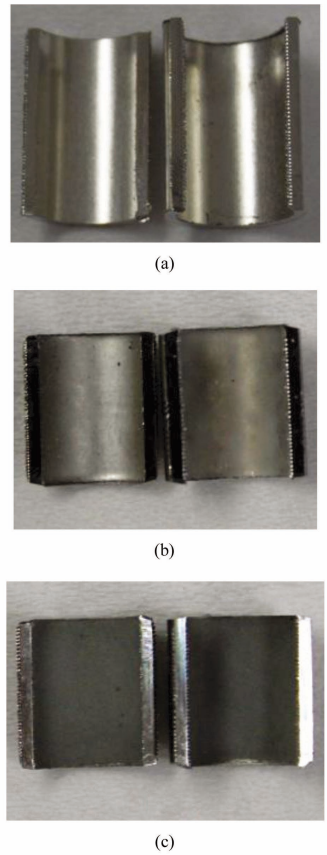

Fig. 9. Macroscopic Observations of the Inner Surface of the Test Section after the CHF Experiments: (a) Water, (b) Al_2O_3/Water Nanofluid, and (c) SiC/Water Nanofluid.

Table 1. Comparison of the CHF Enhancement Ratios in the Flow Boiling Experiment using the Al_2O_3/Water Nanofluid.

Mass flux (kg/m^{2}s)	KAIST (Kim et al. [7])	UNIST
100	1.70	1.06
200	1.60	1.15

the Al_2O_3/water nanofluid, the maximum CHF enhancement ratio was 15 % at an inlet temperature of 50 °C and mass flux of 200 kg/m^{2}s; the maximum CHF enhancement ratio was 41 % at an inlet temperature of 25 °C and mass flux of 150 kg/m^{2}s for the SiC/water nanofluid. For the Al_2O_3/water nanofluid, Kim et al. [7] performed flow boiling CHF experiments at various inlet temperatures (50 and 75 °C) and mass fluxes (100, 200, and 300 kg/m^{2}s) in round tubes with an inner diameter of 0.01041 m and a length of 0.5 m. The experimental conditions of the inlet temperature of 50 °C and mass fluxes of 100 and 200 kg/m^{2}s were the same as the conditions of the experiment presented in this study. However, the CHF enhancement ratios of the Al_2O_3/water nanofluid differed as shown in Table 1. The reason for the difference results from the deposition structure of the nanoparticles being different. Although the flow boiling CHF experiments using the Al_2O_3/water nanofluid have been performed in other studies, comparison was not possible due to the different shape of the test section.

The CHF results for nanofluids were higher than those for water due to the enhanced wettability of the liquid film on the heater surface resulting from the nanoparticle deposition. The nanoparticle deposition occurred as the local dryout occurred. This cause has been stated in numerous previous studies [5-7, 12, 20-23]. The macroscopic observations reveal the deposition of nanoparticles on the inner surface of the test section, as shown in Fig. 9. Furthermore, as seen in Fig. 10, the SEM observations revealed more detail of the nanoparticle deposition. While the research results on the CHF enhancement using nanofluids in flow boiling have been reported, there have not yet been reports on the cause of the CHF enhancement for each nanofluid. In all experiment conditions, the CHF results for the SiC/water nanofluid were more enhanced than those for the Al_2O_3/water nanofluid because the thermal conductivity of SiC nanoparticles is higher than that of Al_2O_3 nanoparticles, as seen in Table 2; furthermore, the deposition structure of the nanoparticles differs, as seen in Fig. 10. Also, as seen in Fig. 11, the contact angle in the

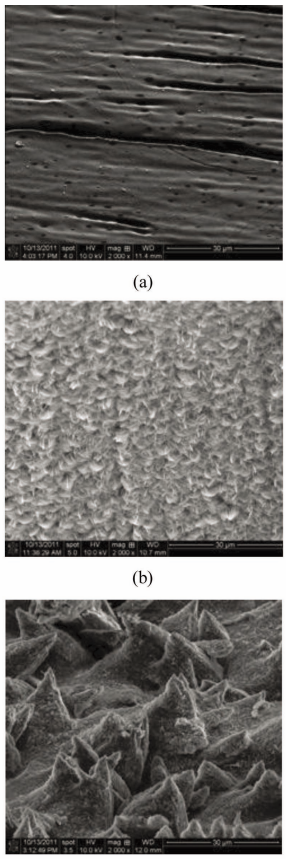

(a)

(b)

(c)

Fig. 10. SEM Observations of the Inner Surface of the Test Section after the CHF Experiments: (a) Water, (b) Al_2O_3/Water Nanofluid, and (c) SiC/Water Nanofluid.

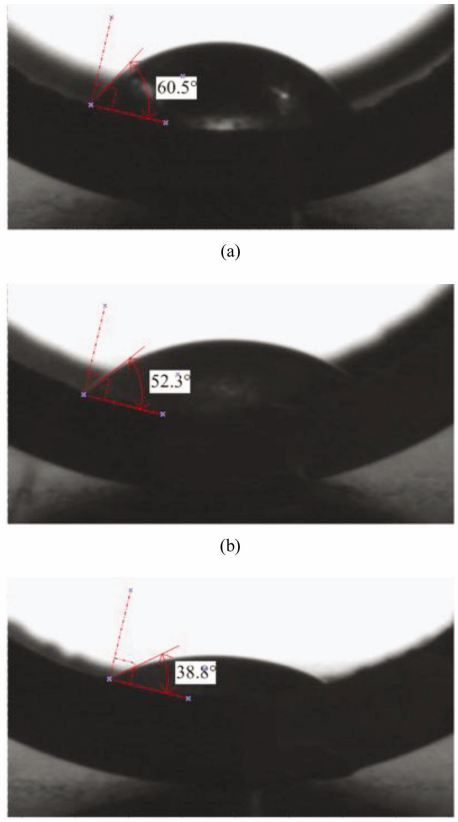

(a)

(b)

(c)

Fig. 11. Contact Angles of the Inner Surface of the Test Section after the CHF Experiments: (a) Water (60.5°), (b) Al_2O_3/Water Nanofluid (52.3°), and (c) SiC/Water Nanofluid (38.8°).

Table 2. Thermal Conductivity of the Nanoparticles.

Nanoparticles	Thermal conductivity (W/mK)
Al_2O_3	40
SiC	490

inner surface of the test section after the CHF experiment using the SiC/water nanofluid (38.8°) was smaller than that after the CHF experiment with water (60.5°) and Al_2O_3/water nanofluid (52.3°) after injecting 10 μl of water. These results demonstrated that the nanoparticle deposition increased the surface wettability.

4. CONCLUSIONS

The following conclusions can be made as a result of the experiments.

(1)In a comparison with the results in the 2006 Groeneveld look-up table, the CHF results for water were found to be similar.

(2)Although the differential pressure increased as the mass flux increased, the CHF of the nanofluids was enhanced regardless of the pressure because the differential pressure was nearly identical according to the increase of the mass flux.

(3)The maximum CHF enhancement of the Al_2O_3/water nanofluid was 15% at an inlet temperature of 50 °C and a mass flux of 200 kg/m^{2}s.

(4)The maximum CHF enhancement of the SiC/water nanofluid was 41% at an inlet temperature of 25 °C and a mass flux of 150 kg/m^{2}s.

(5)The CHF enhancements of the nanofluids caused enhanced wettability of the liquid film on the heater surface due to the nanoparticle deposition. This was confirmed through SEM observations.

(6)The CHF results for the SiC/water nanofluid were more enhanced than those of the Al_2O_3/water nanofluid because the thermal conductivity of the SiC nanoparticles is higher than that of the Al_2O_3 nanoparticles and the deposition structure of the nanoparticles also differs. Furthermore, the contact angle in the inner surface of

the test section after the CHF experiment with the SiC/water nanofluid was smaller than that after the CHF experiment with water and Al_2O_3/water nanofluid. Therefore, the surface wettability, which is important in enhancing the CHF, is increased.

NOMENCLATURE

D Tube diameter (m)
G Mass flux (kg/m^{2}s)
h Latent heat (MJ/kg)
I Measured current (A)
L Length of test section (m)
P Pressure (kPa)
q" Critical heat flux (MW/m^2)
T Temperature (°C)
V Measured voltage (V)
X Steam quality
z Tube length (m)

Subscripts

cr Critical
fg Vaporization
in Inlet
ini Initial
sub Subcooling

ACKNOWLEDGEMENTS

This work was supported by the Nuclear Energy Research Program through the National Research Foundation of Korea (NRF) funded by the Ministry of Education, Science and Technology (MEST) and by a Human Resources Development of the Korea Institute of Energy Technology Evaluation and Planning (KETEP) grant funded by the Korean government Ministry of Knowledge Economy (No. 20114030200010).

REFERENCES

[1] S. H. Chang, Y. H. Jeong, and B. S. Shin, "Critical Heat Flux Enhancement," *Nucl. Eng. Technol.*, vol. 38, pp. 753-762 (2006)
[2] S. U. S. Choi, "Nanofluid: From Vision to Reality through Research," *Journal of Heat Transfer*, vol. 131, 033106 (9 pages) (2006)
[3] S. H. Chang, W. Baek, and T. M. Bae, "A Study of Critical Heat Flux for Low Flow of Water in Vertical Round Tubes under Low Pressure," *Nucl. Eng. Design*, vol. 132, pp. 225-237 (1991)
[4] H. C. Kim, W. Baek, S. H. Chang, "Critical Heat Flux of Water in Vertical Round Tubes at Low Pressure and Low Flow Conditions," *Nucl. Eng. Design*, vol. 199, pp. 49-73 (2000)
[5] S. J. Kim, T. McKrell, J. Buongiorno, and L. Hu, "Alumina Nanoparticles Enhance the Flow Boiling Critical Heat Flux of Water at Low Pressure," *Journal of Heat Transfer*, vol. 130, pp. 044501 (3 pages) (2008)
[6] S. J. Kim, T. McKrell, J. Buongiorno, and L. Hu, "Experimental Study of Flow Critical Heat Flux in Alumina-Water, Zinc-Oxide-Water, and Diamond-Water Nanofluids," *Journal of Heat Transfer*, vol. 131, pp. 043204 (7 pages) (2009)
[7] T. I. Kim, Y. H. Jeong, and S. H. Chang, "An Experimental Study on CHF Enhancement in Flow Boiling using Al2O3 Nano-fluid," *Int. J. Heat Mass Transfer*, vol. 53, pp. 1015-1022 (2010)
[8] D. C. Groeneveld, L. K. H. Leung, P. L. Kirillov V. P. Bobkov, I. P. Smogalev, V. N. Vinogradov, X. C. Huang, and E. Royer, "The 1995 Look-up Table for Critical Heat Flux in Tubes," *Nucl. Eng. Design*, vol. 163, pp. 1-24 (1996)
[9] K. Ahn, "Comparison of Silicon Carbide and Zircaloy4 Cladding during LBLOCA," MIT, Department of Nuclear Engineering (2006)
[10] D. C. Groeneveld, J. Q. Shan, A. Z. Vasic, L. K. H. Leung, A. Durmayaz, J. Yang, S. C. Cheng, and A. Tanase, "The 2006 CHF Look-up Table," *Nucl. Eng. Design*, vol. 237, pp. 1909-1922 (2007)
[11] S. W. Lee, S. D. Park, S. Kang, I. C. Bang, and J. H. Kim, "Investigation of Viscosity and Thermal Conductivity of SiC Nanofluids for Heat Transfer Applications," *Int. J. Heat Mass Transfer*, vol. 54, pp. 433-438 (2011)
[12] V. Saeid and W. Dongsheng, "Critical heat flux (CHF) of Subcooled Flow Boiling of Alumina Nanofluids in a Horizontal Microchannel," *Journal of Heat Transfer*, vol. 132, pp. 102404 (7 pages) (2010)
[13] P. B. Whalley, *Two-Phase Flow and Heat Transfer*, pp. 4-11, Oxford University Press, Oxford New York Tokyo (1996)
[14] O. Baker, "Design of Pipelines for the Simultaneous Flow of Oil and Gas," *Fall Meeting of the Petroleum Branch of AIME*, Dallas, Texas, Oct. 19-21, 1953
[15] G, F. Hewitt and D. N. Roberts, "Studies of Two Phase Flow Patterns by Simultaneous X-ray and Flash Photography," AERE-M2159 (1969)
[16] Y. Taitel and A. E. Dukler, "A Model for Predicting Flow Regime Transitions in Horizontal and Near Horizontal gas-liquid flow," AIChE J., vol. 22, pp. 47-55 (1976)
[17] J. G. Collier and J. R. Thome, *Convective Boiling and Condensation*, 3 rd ed., pp. 329-367, Oxford University Press, Oxford (1994)
[18] A. E. Bergles, "Burnout in Boiling Heat Transfer, Part II: Subcooled and Low Quality Forced Convection Systems," *Nucl. Safety*, vol. 18, pp. 154-167 (1977)
[19] S. K. Moon, W. Baek, and S. H. Chang, "Parametric Trends Analysis of the Critical Heat Flux Based on Artificial Neural Networks," *Nucl. Eng. Design*, vol. 163, pp. 29-49 (1996)
[20] M. S. Sarwar, Y. H. Jeong, and S. H. Chang, "Subcooled Flow Boiling CHF Enhancement with Porous Surface Coatings," *Int. J. Heat Mass Transfer*, vol. 50, pp. 3649-3657 (2007)
[21] I. C. Bang and S. H. Chang, "Boiling heat transfer performance and phenomena of Al_2O_3-water nano-fluids from a plain surface in a pool," *International Journal of Heat and Mass Transfer*, vol. 48, pp. 2407-2419 (2005)
[22] I. C. Bang and J. H. Kim, "Thermal-fluid characterizations of ZnO and SiC nanofluids for advanced nuclear power plants," *Nuclear technology*, vol. 170, no. 1, pp 16-27 (2010)
[23] I. C. Bang, J. H. Jeong, "Nanotechnology for advanced nuclear thermal-hydraulics and safety: boiling and condensation," *Nuclear Engineering and Technology*, vol. 43, no. 3, pp. 217-242 (2011)